

OxiMA: A Frequency-Domain Approach to Address Motion Artifacts in Photoplethysmograms for Improved Estimation of Arterial Oxygen Saturation and Pulse Rate

J. Harvey, S. M. A. Salehizadeh, Y. Mendelson¹, and K. H. Chon²

Abstract—Objective: The purpose of this paper is to demonstrate that a new algorithm for estimating arterial oxygen saturation can be effective even with data corrupted by motion artifacts (MAs). **Methods:** OxiMA, an algorithm based on the time-frequency components of a photoplethysmogram (PPG), was evaluated using 22-min datasets recorded from 10 subjects during voluntarily-induced hypoxia, with and without subject-induced MAs. A Nellcor OxiMax transmission sensor was used to collect an analog PPG while reference oxygen saturation and pulse rate (PR) were collected simultaneously from an FDA-approved Masimo SET Radical RDS-1 pulse oximeter. **Results:** The performance of our approach was determined by computing the mean relative error between the PR/oxygen saturation estimated by OxiMA and the reference Masimo oximeter. The average estimation error using OxiMA was 3 beats/min for PR and 3.24% for oxygen saturation, respectively. **Conclusion:** The results show that OxiMA has great potential for improving the accuracy of PR and oxygen saturation estimation during MAs. **Significance:** This is the first study to demonstrate the feasibility of a reconstruction algorithm to improve oxygen saturation estimates on a dataset with MAs and concomitant hypoxia.

Index Terms—Motion artifacts, oxygen saturation monitoring, hypoxia, pulse rate monitoring, photoplethysmogram, PPG, pulse oximetry, signal processing.

I. INTRODUCTION

VITAL signs and clinical symptoms have been shown to be poor predictors of hypoxia, and in order to justify oxygen therapy, measurement of arterial oxygen saturation by pulse oximetry is being increasingly recommended [1]. Arterial oxygen saturation reflects the relative amount of oxyhemoglobin in the arterial blood. Pulse oximetry is the most common method to

Manuscript received June 19, 2017; revised October 8, 2017, January 2, 2018, and March 7, 2018; accepted May 5, 2018. Date of publication May 17, 2018; date of current version January 18, 2019. This work was supported in part by the U.S. Army Medical Research and Materiel Command (USAMRMC) under Grant W81XWH-12-1-0541. (Corresponding author: K. H. Chon.)

J. Harvey and Y. Mendelson are with the Worcester Polytechnic Institute.

S. M. A. Salehizadeh was with the University of Connecticut.

K. H. Chon is with the University of Connecticut, Storrs, CT 06269 USA (e-mail: ki.chon@uconn.edu).

Digital Object Identifier 10.1109/TBME.2018.2837499

measure arterial oxygen saturation (which is then referred to as “SpO₂”), as oxygenated hemoglobin and reduced hemoglobin have significantly different optical absorbance spectra. Specifically, at a red wavelength of about 660 nm, there is a significant difference in light absorbance between reduced (Hb) and oxygenated hemoglobin (HbO₂). A measurement of the percent oxygen saturation of blood is defined as the ratio of the concentration of oxyhemoglobin to the total concentration of hemoglobin present in the blood. Pulse oximetry relies on the principle that PPG fluctuations originate from changes in arterial blood volume caused by each heartbeat, where the total PPG magnitude depends on the amount of arterial blood entering a peripheral vascular bed; the optical absorbance of the blood, skin and tissue; and the wavelength of the light used to illuminate the blood. PPGs can be used to derive not only the SpO₂ and pulse rate (PR), but also other vital physiological information [2]–[5]. Using a pulse oximeter as a multi-purpose vital sign monitor has clinical appeal, since it is familiar to clinicians and comfortable for the patient [6]. In healthy persons, SpO₂ is typically near 98% at sea level. A lower reading indicates a level of hypoxia. SpO₂ readings below 95% are usually a cause for concern, indicating the need for supplemental oxygen therapy. In certain individuals, such as those with chronic respiratory or cardiac diseases, SpO₂ readings below 95% may be considered normal. However, in general, SpO₂ readings between 90% and 95% represent mild hypoxia, while those between 85% and 90% indicate serious hypoxia, and readings below 85% indicate critical hypoxia [7].

Although there are many promising applications for pulse oximeters, currently, they are primarily used on immobile patients. This is because motion artifacts (MAs) result in unreliable SpO₂ and PR estimations [6], [8]–[17]. Clinicians have consequently cited motion artifacts in pulse oximetry as the most common cause of false alarms, loss of signal, and inaccurate readings [18]. Motion artifacts are caused by many phenomena including variations in light coupling between tissues and the sensor, mechanical pulsation of typically non-pulsatile tissue, variations in sensor contact pressure, and mechanical pulsation of arterial blood asynchronous with the true pulse rate.

In practice, MAs are difficult to remove since the corrupted signal component does not have a predefined narrow frequency

band and its frequency spectrum often overlaps with that of the clean PPG [19]. Hence, it is necessary to develop robust algorithms that are capable of reconstructing the motion-corrupted signal and removing MAs.

Several techniques have been described in the literature for MA detection and removal. Some methods are based on adaptive filtering [8], [20]–[22]. In [23], Diab *et al.* applied an adaptive noise filter technique (a ‘correlation canceler’) to reduce undesired components that are in the frequency band of the desired signal, by dynamically changing the filter transfer function. Other techniques are based on the concept of blind source separation (BSS). The concept of BSS is to reconstruct a set of signals from a set of mixed signals which are assumed to contain both the clean and noisy waveforms [6]. Independent component analysis (ICA) [24], canonical correlation analysis (CCA) [25], principle component analysis (PCA) [26], and singular spectrum analysis (SSA) are some of the more popular BSS techniques [6], [27]. In [9], Kim and Yoo proposed the use of a basic ICA algorithm with block interleaving to reduce MAs. Frequency-domain-based ICA was suggested by Krishnan *et al.* [10]. However, the statistical independence or low correlation assumptions in ICA do not hold in a PPG contaminated by MA [11]. Salehizadeh *et al.* [6] introduced a MA removal algorithm using SSA. The idea was to use SSA to decompose the corrupted segment adjacent to the clean segment and choose the SSA components in the corrupted segment that had a similar frequency range to that of the adjoining clean components. Although the algorithm performs well for slowly time-varying dynamic changes, it cannot be applied in scenarios where PR varies quickly, which can occur when a subject is exercising at a rapid pace. Using accelerometer data has also been shown to be helpful in removing MA. For instance, Fukushima *et al.* [12] suggested a spectrum subtraction technique to remove the spectrum of accelerometer data from that of a corrupted PPG. Accelerometer data can also be used to reconstruct the observation model for Kalman filtering [13].

Three noteworthy algorithms recently published for PR estimation during motion and physical activities are TROIKA, JOSS and SpaMA [28]–[30] in which time-frequency spectrum estimation, and spectral peak tracking and verification, are used to estimate and monitor PR during intensive physical activity. All three algorithms make use of both PPG and accelerometer information to obtain an accurate estimation of PR during a treadmill experiment. Although these techniques yield accurate PR estimations during physical activities, SpO₂ estimations were not performed.

In [31]–[33], other techniques were introduced to estimate the blood oxygen saturation from the magnitudes of selected peaks contained in the frequency-domain spectra of the red and infrared PPGs. The method proposed by Athan *et al.* was an approach to estimate SpO₂ from PPG signals in the frequency domain according to the magnitude of the highest peak in the spectrum [35]. This method works well when there are minimal motion artifacts and the PPG signal is robust. Hence, this method is likely to suffer in SpO₂ estimation accuracy when there are significant motion artifacts and the signal quality of the PPG signal is not optimal. The work by Rusch *et al.* exam-

ines the estimation of SpO₂ also using the spectral domain. Specifically, the work examines both the FFT and discrete cosine transformation (DCT) to estimate SpO₂ [33]. The authors reported similar results with both approaches, although in certain instances the FFT method worked better than DCT, and vice versa. However, this work appears to assume that motion artifacts are minimal, hence, both the FFT and DCT methods’ accuracy in estimating SpO₂ may suffer when significant noise is present. The patent by Kaestle *et al.* also proposed a method based on spectral analysis of red and infrared PPG signals to estimate SpO₂ [34]. To account for noise and motion artifacts, the method is designed to look for ten features derived from spectral analysis of PPG. Based on the characteristics of the individual spectral peak features, point scores are assigned. Those spectral peaks with higher point scores are identified as belonging to a blood pulse. However, it is not clear from the patent how one determines the threshold at which point scores indicate that a peak is associated with a blood pulse. It is stated that an average value formulation or historical evaluation are carried out to determine the point score threshold value, but it is left nebulous and thus unclear how the threshold value can be obtained. While this method tries to address noise and motion artifacts, the ten spectral features of the method will vary commensurate with the degree of motion and noise artifacts. Moreover, the point scoring approach for each of the ten features appears to be arbitrary, as it is empirically derived. These approaches by Athan, Rusch, and Kaestle rely on the calculation of SpO₂ using ratios of the magnitudes of individual spectral peaks.

In this paper, a time-frequency based approach is presented to accurately estimate both SpO₂ and PR based on PPG reconstructions: time-domain waveforms that are reconstructed based on the optimal selection of frequency-domain components that are believed to represent these PPGs and not the accompanying motion artifact. The algorithm, termed motion artifact removal for oxygen saturation estimation (OxiMA), is comprised of six distinct stages: 1) time-frequency spectral analysis, 2) signal decomposition, 3) spectral filtering, 4) PR extraction and tracking, 5) signal reconstruction, and 6) SpO₂ estimation. We show in the Results section that the OxiMA algorithm provides accurate PR and SpO₂ estimates even during motion. Other similar algorithms (e.g., TROIKA and JOSS), as noted above, did not demonstrate their ability to obtain SpO₂ estimations, as they were designed for PR estimations in the presence of intense motion artifacts.

II. MATERIALS AND EXPERIMENTS

The OxiMA algorithm was evaluated on a lab-controlled dataset that was recorded during voluntarily-induced hypoxia. In an IRB-approved study (Docket 15-012M, Worcester Polytechnic Institute) which involved 10 subjects, one set of data was collected from each subject for a duration of 22 minutes. Ten males between the ages of 23 and 58 years old were recruited for this study (mean age of 27 years). Reference SpO₂ and PR were collected from an FDA-approved Masimo SET Radical RDS-1 pulse oximeter (mounted on the left hand), while a Nellcor OxiMax sensor (mounted on the right hand) was simul-

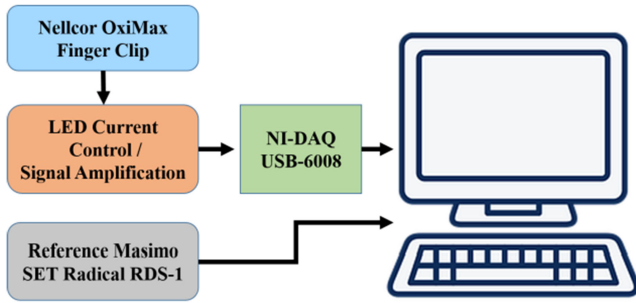


Fig. 1. Data collection flow chart.

TABLE I
EXPERIMENTAL PROTOCOL

Start Time (minutes)	Event	Duration (minutes)	End Time (minutes)
0	Rest (Baseline)	2	2
2	Bag Breathing (No Motion)	2	4
4	Rest (Oxygen Recovery)	1	5
5	Rest	2	7
7	Bag Breathing (Motion)	2	9
9	Rest (Oxygen Recovery)	1	10
10	Rest	2	12
12	Bag Breathing (No Motion)	2	14
14	Rest (Oxygen Recovery)	1	15
15	Rest	2	17
17	Bag Breathing (Motion)	2	19
19	Rest (Oxygen Recovery)	1	20
20	Rest	2	22

taneously used to collect an analog PPG signal (see Fig. 1). A National Instruments NI USB-6008 12-bit, multifunction I/O, data acquisition system was used to acquire and digitize the analog PPG signal at a rate of 512 samples per second. The AC (time-varying) and DC (baseline) components of the PPGs were obtained via MATLAB by filtering the red (R) and infrared (IR) composite PPGs with 4th-order band-pass (0.5–12 Hz) and low-pass (0.5 Hz cutoff frequency) zero-phase digital filters, respectively.

The protocol for this experiment is presented in Table I. Each subject sat in a chair and was asked to rebreathe into a 1-gallon bag for four two-minute intervals. Each interval was followed by a 1-minute rest period and then a 2-minute rest period. During the first and third times the subject rebreathed into the bag, they were asked to remain still. During the second and fourth times the subject rebreathed into the bag, they were asked to

TABLE II
OXiMA ALGORITHM: PR AND SPO₂ ESTIMATION**Stage 1. Time-Frequency Spectral Analysis**

- 1.1. Downsample PPG from the original sampling frequency of 512 Hz to 20 Hz.
- 1.2. Compute the VFCDM based time-frequency spectrum (TFS).

Stage 2. Signal Decomposition

- 2.1. Decompose the PPG into its frequency components according to frequency bands in the TFS.

Stage 3. Spectral Filtering

- 3.1. Consider PR to be in the range of [0.5 Hz – 3 Hz].
- 3.2. Assume that the largest two peaks and their corresponding frequencies in the filtered PPG spectrum can provide PR information.

Stage 4. Pulse Rate Tracking and Extraction

- Case (1): Determine if the largest frequency component is within 10 bpm of the previous PR. If not, proceed to case (2).
- Case (2): Determine if the second largest frequency component is within 10 bpm of the previous PR. If not, proceed to case (3).
- Case (3): Determine if the PR cannot be extracted from the spectrum and in this case use the previous PR, or, for offline implementation, cubic spline interpolation can be applied to fill in the missing PR information.

Stage 5. PPG Reconstruction

- 5.1. Reconstruct the PPG using the summation of VFCDM components with frequencies closest to the selected PR during each window. That is, use only the components within the anticipated PR range.

Stage 6. Oxygen Saturation Estimation

- 6.1. Calculate SpO₂ estimations from reconstructed infrared and red PPGs using the following empirical calibration equation:

$$SpO_2(\%) = 110 - 25R$$

where

$$R = \frac{AC_{Red}/DC_{Red}}{AC_{IR}/DC_{IR}}$$

introduce motion artifacts into the measurement. The motion performed was typically excessive flexion and extension of the wrist and digits. Subjects were not instructed to move in any particular way, but it was observed that flexion and extension seemed easiest for subjects. Each subject wore a disposable nose clip to prevent accidental breathing of room air. The Masimo reference sensor placed on the left hand remained motionless for the entire duration of the study. The PPG signal from this sensor was collected without motion in order to be a clean reference signal to use for comparison with the reconstructed PR and SpO₂ estimations using the proposed algorithm. Subjects had at least two minutes of rest between successive breathing maneuvers, with more time if requested. An informed consent was required of each subject prior to data recording.

This sequence of data allowed us to test the efficacy of the OxiMA algorithm while a subject experienced different levels of short term hypoxia accompanied by motion artifacts. For reference, other clinical studies showed that SpO₂ levels in patients suffering from mild to moderate sleep apnea can drop to about 80% for short periods of time (23–70 sec) without irreversible physiological effects [34].

III. METHODOLOGY

The procedure for the OxiMA algorithm is presented in Table II. Details of each stage will be described in Section III-A through Section III-F.

TABLE III
VFCDM ALGORITHM PROCEDURE

Consider a sinusoidal signal $x(t)$ to be a narrow-band oscillation with a time-varying modulating frequency $f(\tau)$, instantaneous amplitude $A(t)$, phase $\phi(t)$, and low frequency component $dc(t)$:

$$x(t) = dc(t) + A(t) \cos\left(\int_0^t 2\pi f(\tau) d\tau + \phi(t)\right) \quad (i)$$

Step (1) We can extract the instantaneous amplitude information $A(t)$ and phase information $\phi(t)$ by first multiplying (i) by $e^{-j\int_0^t 2\pi f(\tau) d\tau}$ which results in the following:

$$\begin{aligned} z(t) &= x(t)e^{-j\int_0^t 2\pi f(\tau) d\tau} \\ &= dc(t)e^{-j\int_0^t 2\pi f(\tau) d\tau} + \left(\frac{A(t)}{2}\right)e^{j\phi(t)} \\ &\quad + \left(\frac{A(t)}{2}\right)e^{-j\left(\int_0^t 4\pi f(\tau) d\tau + \phi(t)\right)} \end{aligned} \quad (ii)$$

Step (2) If $z(t)$ is filtered with an ideal low-pass filter (LPF) with a cutoff frequency $f_c < f_0$, where f_0 is the center frequency of interest, then the filtered signal $z_{lp}(t)$ will contain only the component of interest:

$$z_{lp}(t) = \frac{A(t)}{2} e^{j\phi(t)}$$

Step (3) By changing the center frequency, followed by using the variable frequency approach as well as the LPF, the signal, $x(t)$, can be decomposed into sinusoidal modulations, d_i , by the variable frequency complex demodulation technique as follows:

$$\begin{aligned} x(t) &= \sum_i d_i \\ &= dc(t) + \sum_i A_i(t) \cos\left(\int_0^t 2\pi f_i(\tau) d\tau + \phi_i(t)\right) \end{aligned} \quad (iii)$$

Step (4) The instantaneous amplitude, phase, and frequency of $x(t)$ in (iii) can be calculated using the Hilbert transform:

$$Y(t) = \text{imag}\left(z_{lp}(t)\right) = H[X(t)] = \frac{1}{\pi} \int \frac{X(t')}{t-t'} dt'$$

$$X(t) = \text{real}\left(z_{lp}(t)\right)$$

$$A(t) = 2|z_{lp}(t)| = \sqrt{X^2(t) + Y^2(t)} \quad (iv)$$

$$\phi(t) = \arctan\left(\frac{\text{imag}\left(z_{lp}(t)\right)}{\text{real}\left(z_{lp}(t)\right)}\right) = \arctan\left(\frac{Y(t)}{X(t)}\right) \quad (v)$$

$$f(t) = f_0 + \frac{1}{2\pi} \frac{d\phi(t)}{dt} \quad (vi)$$

A. Time-Frequency Spectral Analysis

In order to compute the time-frequency spectrum, a variable frequency complex demodulation (VFCDM) technique was adopted [35]. Table III presents the VFCDM procedure.

By taking a K-second window of the PPG, computing the VFCDM spectrum of the windowed segment, and then sliding the window along the entire dataset, we can estimate a time-varying spectrum. There is no overlap between the sliding time windows. The window segment length, K, is set to 8 seconds and is shifted by 8 seconds. As an example, the IR PPG, an 8-second window of the IR PPG, and the resultant VFCDM time-frequency spectrum of recording #6 are represented in

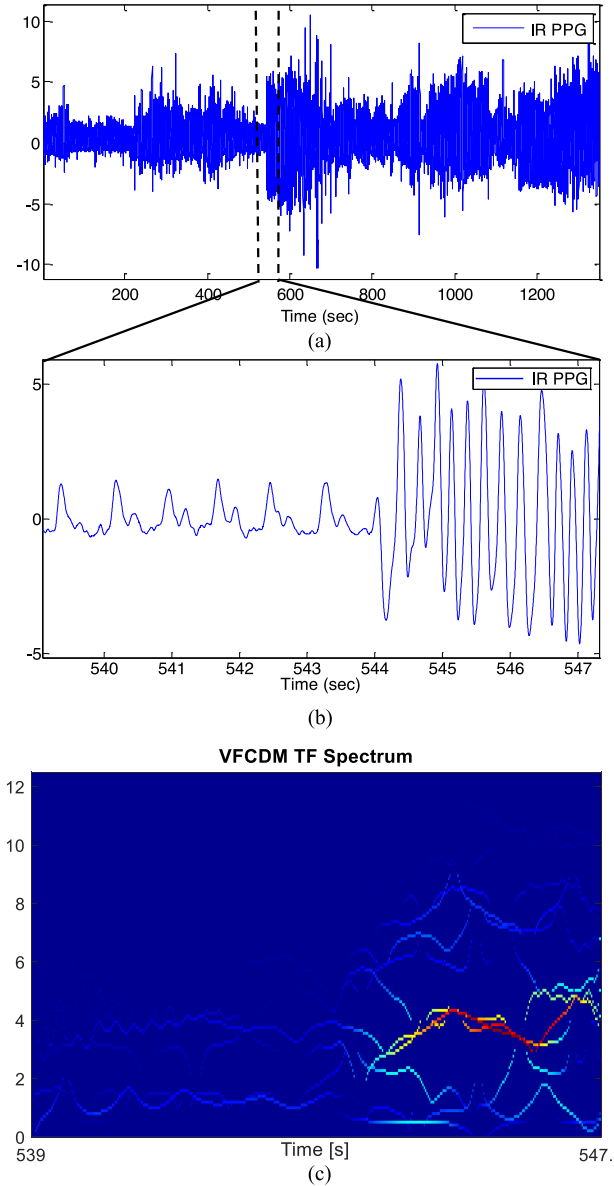


Fig. 2. Time- and frequency-domain representations for recording #6. (a) Infrared PPG. (b) Zoomed-in PPG. (c) VFCDM TF spectrum of the PPG shown in (b).

Fig. 2. The next section details how the PPGs are decomposed into their frequency components using VFCDM.

B. Signal Decomposition

We can now decompose the original PPG into sinusoidal modulations using VFCDM (see Table III):

$$\begin{aligned} x(t) &= \sum_{i=1}^N \text{Component}\{i\} \\ &= dc(t) + \sum_{i=1}^N A_i(t) \cos(2\pi f_i(t) + \phi_i(t)) \end{aligned} \quad (1)$$

where $dc(t)$ is the DC term, and $A_i(t)$, $f_i(t)$ and $\phi_i(t)$ are instantaneous amplitude, frequency, and phase calculated from step (4) in Table III. We can thus decompose the PPG using the

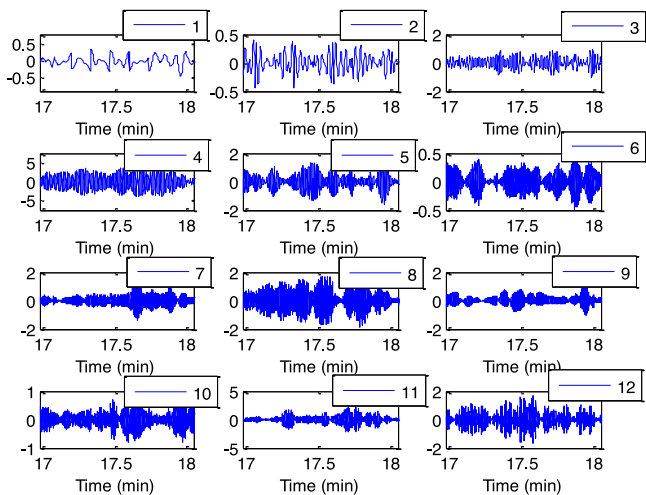


Fig. 3. VFCDM signal decomposition of recording #6 (zoomed-in one min segments). The twelve components are obtained from the IR PPG.

VFCDM procedure into 12 components that cover $N = 12$ fixed frequency bands, each with a distinct central frequency. Fig. 3 shows the twelve components decomposed from the IR PPG for a representative subject; 12 components are also obtained from the red PPG but are not shown.

Among the twelve frequency bands, bands 1 through 5 correspond to the frequency range of [0.5 Hz to 3 Hz], which typically encompasses the true PR, accounting for both reduced and elevated pulse rates.

The next step is to determine which components out of these 5 candidates' frequencies should be chosen to reconstruct the signal so that the most accurate estimation of PR and SpO_2 can be obtained. The subsequent sections *C* through *F* detail our strategies to optimally select frequencies, estimate PRs, and reconstruct the PPGs so that more accurate SpO_2 estimates can be made.

C. Spectral Filtering

After obtaining the power spectral density during each window, the PR is assumed to be confined to the range [0.5 Hz–3 Hz], which takes into account both at-rest and high PR values due to either tachycardia or exercise. Next, for PR estimation, the strategy is to keep only those frequencies that correspond to the highest and second-highest peaks in each column of the time-frequency spectrum (TFS) matrix. This and the next steps of OxiMA are adopted from our previously-developed algorithm SpaMA [30]. The main difference here is that the procedure is implemented on the VFCDM time-frequency matrix for each segmented window.

In general, the PR component in the spectrum of the PPG for each window can relate to one of three possible cases: (1) the PPG quality is good and is devoid of motion and noise artifacts, (2) the PPG is misshapen but the true PR component is mostly present, and (3) the true PR component is weak or absent. For the ideal case (1), the PR can be extracted and is represented by the largest frequency component in the PPG spectrum. For case (2), the PR component's spectral power is smaller than the motion

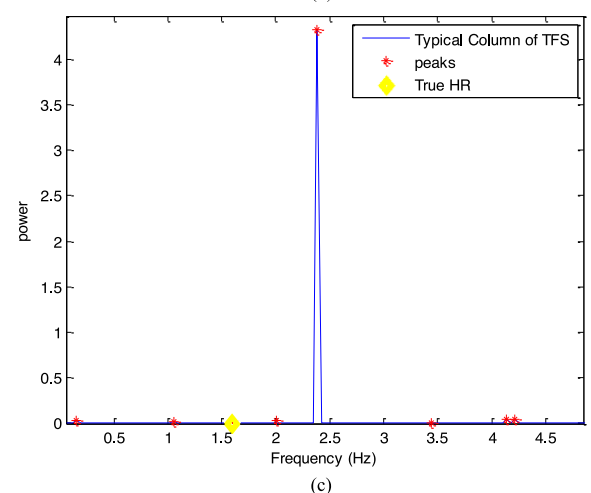
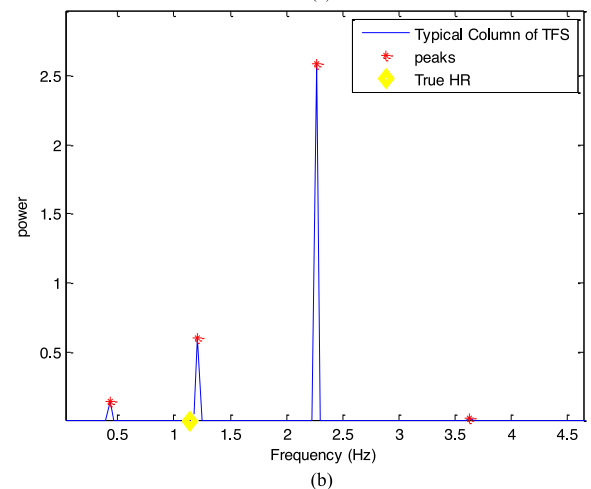
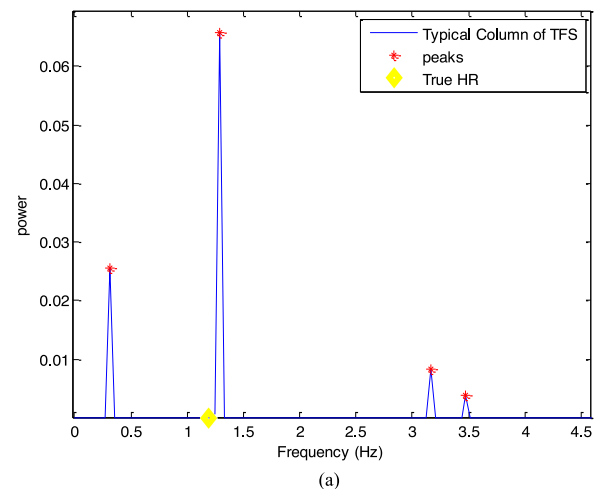


Fig. 4. Three possible cases of PR estimation. (a) True PR is close to the highest peak of the spectrum. (b) True PR is close to the second highest peak in the spectrum. (c) True PR is not close to any of the prominent peaks in the spectrum.

component's spectral power, and the frequency related to the second highest peak in the spectrum is interpreted as the true PR. In case (3), the missing PR value can be interpolated using the cubic spline approach, assuming that the motion artifacts are short lasting. Fig. 4 depicts the above three cases. In Fig. 4(a)

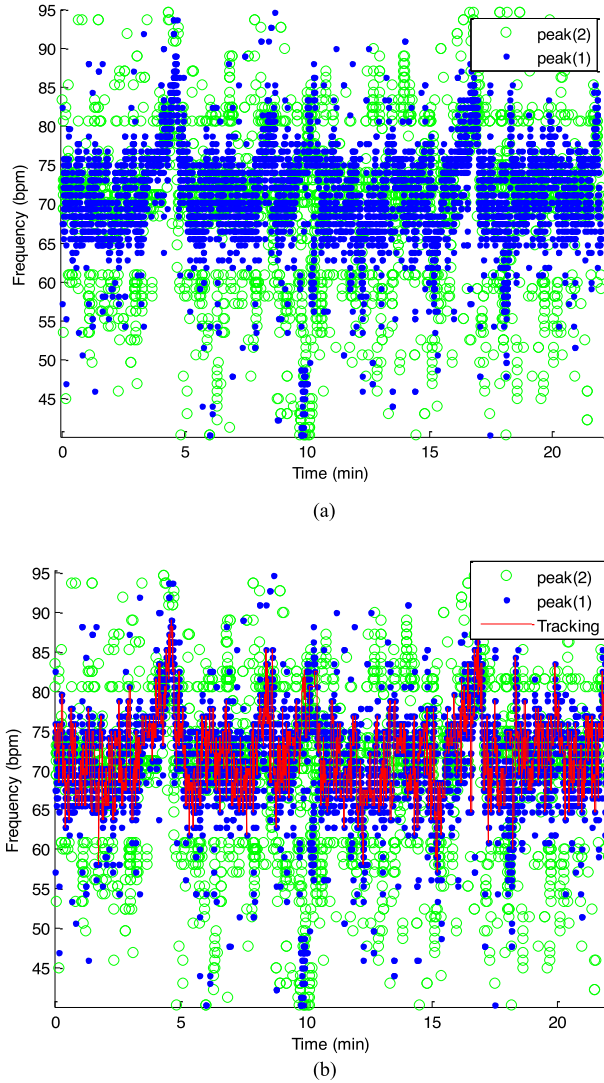


Fig. 5. PR Extraction (recording #6). (a) PR from the first and second prominent components of each spectrum for the TFS shown in Fig. 2(c); Blue dots and green circles represent the first and second highest peaks in the spectrum, respectively. (b) PR extraction from the processed TFS.

and (b), the true PR is close to the highest or second-highest peak respectively, while in Fig. 4(c), the true PR is far from the dominant peak(s) in the spectrum. We can assume that as long as the PPG data are clean, the PR equals the frequency component with the highest power (peak) in each column of the TFS matrix. When the data are corrupted by MAs, the PR may not be represented by the largest frequency component, but rather by the second-largest. In the worst case (3), the dominant frequencies are no longer associated with the expected pulse rate at all.

The first step of the spectral filtering procedure is to select only the two largest spectral peaks and their associated frequencies in each column of the TFS. Hence, the original TFS (Fig. 2(c)) can be processed to select only the two largest spectral peaks (see Fig. 5). This step in the OxiMA algorithm involves retaining only the two largest frequency peaks (during each time window) that fall within the defined PR range (30–180 bpm).

D. Pulse Rate Tracking and Extraction

The next step after processing the TFS is the extraction of PR. The PR tracking procedure is as follows. Assuming that we have knowledge of the initial PR, the PR during each window is extracted by comparing the frequencies of the spectral peaks to the previous PR value [30].

If the largest peak is within 10 bpm of the previous PR value ($PR_{k-1} \pm 10$), it is chosen; if not, we check whether or not the second largest peak is within the 10 bpm range. If the PR value deviates by more than 10 bpm, the PR from the previous window is used. Fig. 5(b) illustrates the tracking of PR based on this procedure.

E. PPG Reconstruction

After PR values during each time window are estimated from the time-frequency spectrum, the signal reconstruction step of the OxiMA algorithm is performed. Once the red and infrared PPGs are reconstructed, more accurate estimates of SpO_2 can be made.

Given the estimated PR values for each 8-sec window as detailed in the preceding sections C through D, we now reconstruct the time-domain signal $x(t)$ as denoted in (1) using only the first five components as described in Section III-B. This reconstructed signal will improve the accuracy of SpO_2 estimations. We assume that the reconstructed signal is dominated by the true PR, thus, represents the true PPG.

F. Oxygen Saturation Estimation

In order to accurately estimate SpO_2 , red and infrared PPGs with clearly separable DC and AC components are required. Let the pulsatile components of the red and infrared PPG be denoted as AC_{Red} and AC_{IR} , and let the baseline components be denoted as DC_{Red} and DC_{IR} , respectively. Then, the ‘ratio-of-ratios’ is defined as [19], [20]:

$$R = \frac{AC_{Red}/DC_{Red}}{AC_{IR}/DC_{IR}} \quad (2)$$

SpO_2 is then estimated according to the following empirical linear approximation given by [33]:

$$SpO_2 (\%) = 110 - 25R \quad (3)$$

Fig. 6(e) represents the estimated SpO_2 values obtained from the OxiMA reconstructed signal in comparison to the reference Masimo SpO_2 values and the estimated SpO_2 prior to signal reconstruction.

Relative error and error percentage were used to show the performance of OxiMA. The two performance metrics are defined as:

$$E_1^* = \mu_{error} \pm \sigma_{error} \quad (4)$$

$$E_2^* = \frac{1}{W} \sum_{k=1}^W \frac{error(k)}{Feature_{ref}(k)} \times 100\% \quad (5)$$

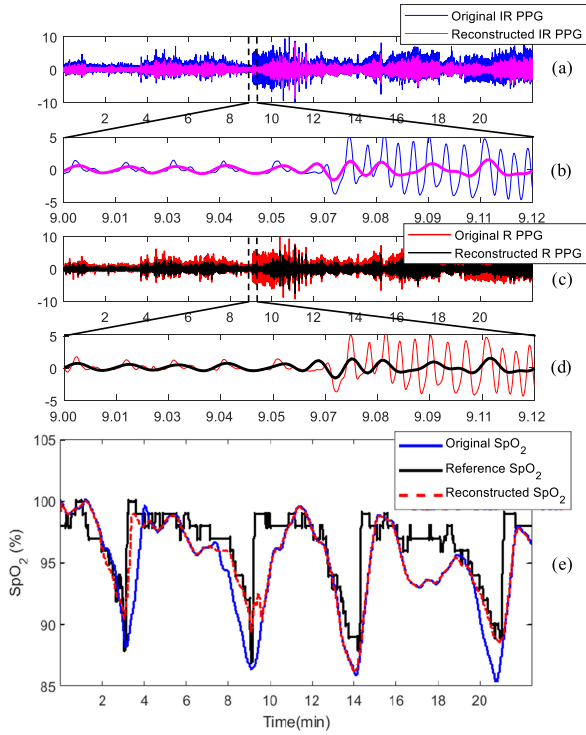


Fig. 6. PPG reconstruction and SpO₂ estimation (recording #6). (a) Original (blue) and reconstructed (magenta) infrared PPG. (b) Zoomed-in version of (a). (c) Original (red) and reconstructed (black) red PPG. (d) Zoomed-in version of (c). (e) Comparison of reference SpO₂ vs. original and reconstructed SpO₂.

where,

$$\begin{aligned} \text{error}(k) &= |Feature^*(k) - Feature^*_{ref}(k)| \\ \mu_{error} &= \frac{1}{W} \sum_{k=1}^W \text{error}(k) \\ \sigma_{error} &= \sqrt{\frac{1}{W} \sum_{k=1}^W (\text{error}(k) - \mu_{error})^2} \end{aligned}$$

where E_1^* is relative error, E_2^* is percent error, $Feature^*$ is the estimated feature (PR or SpO₂), and W is the number of motion- and noise-corrupted windows. The relative error and percent error were calculated pre- and post-application of the OxiMA algorithm, where for the pre-application data we have taken the raw PPG signal and applied (2) and (3). Improvement from pre- to post-application of the OxiMA algorithm can be calculated as:

$$ImRate(\%) = E_2^{Original} - E_2^{OxiMA} \quad (6)$$

IV. RESULTS

Tables IV and V represent the error [$E_1^{Original}, E_1^{OxiMA}$] and the error percentage [$E_2^{Original}, E_2^{OxiMA}$] of PR and SpO₂ for the varying hypoxia dataset during the finger movement period. The performance of the OxiMA algorithm is evaluated, where both with- and without-reconstruction estimations are compared to the reference PR and SpO₂ values obtained from the Masimo pulse oximeter.

TABLE IV
OXiMA ALGORITHM PERFORMANCE (PR ESTIMATES DURING MOTION)

Subject	Original PR estimation error		OxiMA PR estimation error	
	E_1	E_2 (%)	E_1	E_2 (%)
1	7.10±3.0	9.58	2.16±1.1	2.80
2	9.62±2.4	10.92	2.97±2.5	4.10
3	13.38±2.9	14.44	2.01±0.7	2.37
4	7.14±3.3	8.31	2.72±1.4	3.44
5	20.53±7.2	26.96	7.89±5.7	10.18
6	6.44±2.8	8.22	1.66±1.3	2.41
7	19.41±6.8	24.65	3.38±1.8	4.41
8	6.45±2.7	7.93	2.52±0.6	2.77
9	6.10±2.4	7.13	2.84±0.5	2.95
10	5.94±2.5	7.11	2.11±0.6	2.33
mean±std	10.21±3.6	12.52±7.3	3.02±1.6	3.8±2.4

TABLE V
OXiMA ALGORITHM PERFORMANCE (SpO₂ ESTIMATES DURING MOTION)

Subject	Original SpO ₂ estimation error		OxiMA SpO ₂ estimation error	
	E_1	E_2 (%)	E_1	E_2 (%)
1	4.44±2.0	4.46	1.44±1.3	1.73
2	12.56±5.4	13.47	4.01±0.9	4.33
3	10.33±4.1	12.91	3.70±0.4	3.93
4	4.58±4.6	7.28	1.83±1.5	2.31
5	15.92±6.8	18.13	5.39±3.8	6.79
6	3.90±4.4	4.77	2.24±1.1	2.61
7	9.41±3.9	10.35	4.61±2.7	5.88
8	6.43±3.1	8.58	3.12±0.9	3.49
9	3.74±3.4	5.37	3.41±0.8	3.93
10	8.14±6.4	11.97	3.65±1.2	4.10
mean±std	7.94±4.41	9.73±4.5	3.24±1.5	3.91±1.5

TABLE VI
OXiMA ALGORITHM PERFORMANCE COMPARISON
(ESTIMATES DURING MOTION)

Subject	PR Improvement (%)	SpO ₂ Improvement (%)
1	6.78	2.73
2	6.82	9.14
3	12.07	8.98
4	4.87	4.97
5	16.78	11.34
6	5.81	2.16
7	20.24	4.47
8	5.16	5.09
9	4.18	1.44
10	4.78	7.87
mean±std	8.75±5.7	5.82±3.3
median	6.29	5.03

The results presented in Table VI show that OxiMA on average improves PR and SpO₂ estimations by 8.75% and 5.82%, respectively, when compared to those estimations without the reconstruction algorithm.

V. CONCLUSION

In this study, we introduced a technique (OxiMA) to minimize the effects of motion artifacts in PPGs in order to improve the accuracy of SpO₂ and PR estimations. The strategy was to decompose each PPG into frequency bands within the pulse rate range using our previously-developed VFCDM algorithm. In our approach, we take only the decomposed components that are within the pulse rate range, including both extremes of low and high pulse rates, and reconstruct the signal based on these components. This procedure allows the removal of frequencies that are not within the prescribed PR range. From this reconstructed time-series we have demonstrated an improvement in PR/SpO₂ estimations on a dataset containing MAs and concomitant hypoxia. OxiMA may prove useful in improving the repeatability of pulse oximetry estimates in wired and wireless monitoring scenarios that include MAs.

REFERENCES

- [1] M. Laman *et al.*, "Can clinical signs predict hypoxaemia in Papua New Guinean children with moderate and severe pneumonia?," *Ann. Trop. Paediatr.*, vol. 25, no. 1, pp. 23–27, 2005.
- [2] K. H. Chon *et al.*, "Estimation of respiratory rate from photoplethysmogram data using time-frequency spectral estimation," *IEEE Trans. Biomed. Eng.*, vol. 56, no. 8, pp. 2054–2063, Aug. 2009.
- [3] N. Reljin *et al.*, "Tidal volume estimation using the blanket fractal dimension of the tracheal sounds acquired by smartphone," *Sensors (Basel)*, vol. 15, no. 5, pp. 9773–9790, 2015.
- [4] J. W. Chong *et al.*, "Arrhythmia discrimination using a smart phone," *IEEE J. Biomed. Health Inf.*, vol. 19, no. 3, pp. 815–824, May 2015.
- [5] B. Reyes *et al.*, "Tidal volume and instantaneous respiration rate estimation using a smartphone camera," *IEEE J. Biomed. Health Inf.*, vol. 21, no. 3, pp. 764–777, May 2016.
- [6] S. M. Salehizadeh *et al.*, "Photoplethysmograph signal reconstruction based on a novel motion artifact detection-reduction approach. Part II: Motion and noise artifact removal," *Ann. Biomed. Eng.*, vol. 42, no. 11, pp. 2251–2263, 2014.
- [7] R. Tamisier *et al.*, "A new model of chronic intermittent hypoxia in humans: effect on ventilation, sleep, and blood pressure," *J. Appl. Physiol.*, vol. 107, no. 1, pp. 17–24, 2009.
- [8] S. Seyedtabaai and L. Seyedtabaai, "Kalman filter based adaptive reduction of motion artifact from photoplethysmographic signal," *World Acad. Sci. Eng. Tech.*, vol. 37, pp. 173–176, 2008.
- [9] B. S. Kim and S. K. Yoo, "Motion artifact reduction in photoplethysmography using independent component analysis," *IEEE Trans. Biomed. Eng.*, vol. 53, no. 3, pp. 566–568, Mar. 2006.
- [10] R. Krishnan *et al.*, "Two-stage approach for detection and reduction of motion artifacts in photoplethysmographic data," *IEEE Trans. Biomed. Eng.*, vol. 57, no. 8, pp. 1867–1876, Aug. 2010.
- [11] J. Yao and S. Warren, "A short study to assess the potential of independent component analysis for motion artifact separation in wearable pulse oximeter signals," in *Conf. Proc. IEEE Eng. Med. Biol. Soc.*, 2005, vol. 4, pp. 3585–3588.
- [12] H. Fukushima *et al.*, "Estimating heart rate using wrist-type Photoplethysmography and acceleration sensor while running," in *Conf. Proc. IEEE Eng. Med. Biol. Soc.*, 2012, pp. 2901–2904.
- [13] B. Lee *et al.*, "Improved elimination of motion artifacts from a photoplethysmographic signal using a Kalman smoother with simultaneous accelerometry," *Physiol. Meas.*, vol. 31, no. 12, pp. 1585–1603, 2010.
- [14] S. Rhee *et al.*, "Artifact-resistant power-efficient design of finger-ring plethysmographic sensors," *IEEE Trans. Biomed. Eng.*, vol. 48, no. 7, pp. 795–805, Jul. 2001.
- [15] S. H. Kim *et al.*, "Adaptive noise cancellation using accelerometers for the PPG signal from forehead," in *Conf. Proc. IEEE Eng. Med. Biol. Soc.*, 2007, pp. 2564–2567.
- [16] L. R. Mujica-Parodi *et al.*, "Limbic dysregulation is associated with lowered heart rate variability and increased trait anxiety in healthy adults," *Human Brain Mapping*, vol. 30, no. 1, pp. 47–58, 2007.
- [17] J. W. Chong *et al.*, "Photoplethysmograph signal reconstruction based on a novel hybrid motion artifact detection-reduction approach. Part I: Motion and noise artifact detection," *Ann. Biomed. Eng.*, vol. 42, no. 11, pp. 2238–2250, 2014.
- [18] A. Jubran, "Pulse oximetry," *Crit. Care*, vol. 3, no. 2, pp. R11–R17, 1999.
- [19] N. V. Thakor and Y. S. Zhu, "Applications of adaptive filtering to ECG analysis: Noise cancellation and arrhythmia detection," *IEEE Trans. Biomed. Eng.*, vol. 38, no. 8, pp. 785–794, Aug. 1991.
- [20] P. S. R. Diniz, *Adaptive Filtering Algorithms and Practical Implementation*. Boston, MA USA: Springer-Verlag, 2008.
- [21] R. E. Kalman, "A new approach to linear filtering and prediction problems," *J. Basic Eng.*, vol. 82, no. 1, pp. 35–45, 1960.
- [22] F. Morbidi *et al.*, "Application of Kalman filter to remove TMS-induced artifacts from EEG recordings," *IEEE Trans. Control Syst. Technol.*, vol. 16, no. 6, pp. 1360–1366, Nov. 2008.
- [23] M. K. Diab *et al.*, *Signal Processing Apparatus*. U.S. Patent 7,496,393, Masimo Corporation, Irvine, CA, 2009.
- [24] P. Comon, "Independent component analysis, a new concept?," *Signal Process.*, vol. 36, no. 3, pp. 287–314, 1994.
- [25] B. Thompson, *Canonical Correlation Analysis: Uses and Interpretation*. University of South Florida, Tampa, FL: Sage, 1984.
- [26] I. Jolliffe, *Principal Component Analysis*. 2 ed. (Springer Series in Statistics) New York, NY, USA: Springer-Verlag, 2002.
- [27] J. B. Elsner and A. A. Tsonis, *Singular Spectrum Analysis: A New Tool in Time Series Analysis*, 2 ed. New York, NY, USA: Springer, 1996.
- [28] Z. Zhang, Z. Pi, and B. Liu, "TROIKA: A general framework for heart rate monitoring using wrist-type photoplethysmographic signals during intensive physical exercise," *IEEE Trans. Biomed. Eng.*, vol. 62, no. 2, pp. 522–531, Feb. 2015.
- [29] Z. Zhang, "Photoplethysmography-based heart rate monitoring in physical activities via joint sparse spectrum reconstruction," *IEEE Trans. Biomed. Eng.*, vol. 62, no. 8, pp. 1902–1910, Aug. 2015.
- [30] S. M. Salehizadeh *et al.*, "A novel time-varying spectral filtering algorithm for reconstruction of motion artifact corrupted heart rate signals during intense physical activities using a wearable photoplethysmogram sensor," *Sensors (Basel)*, vol. 16, no. 10, pp. 1–20, 2015.
- [31] S. Kaestle *et al.*, *Method and Apparatus for Determining the Concentration of a Component*, Hewlett-Packard Company, Palo Alto, CA, Google Patents, 2000.
- [32] S. P. Athan and J. E. Scharf, *Portable Pulse Oximeter*, University of South Florida, Tampa, FL, Google Patents, 1996.
- [33] T. L. Rusch *et al.*, "Signal processing methods for pulse oximetry," *Comput. Biol. Med.*, vol. 26, no. 2, pp. 143–159, 1996.
- [34] Z. Shi, G. Jin, and T. Li, "Pulse oxyhemoglobin desaturation index for the screening of obstructive sleep apnea syndrome," *Sci. Rep.*, vol. 1, no. 4, 2012.
- [35] H. Wang *et al.*, "A high resolution approach to estimating time-frequency spectra and their amplitudes," *Ann. Biomed. Eng.*, vol. 34, no. 2, pp. 326–338, 2006.